

# A Numerical Analysis to the $\pi$ and $K$ Coupled–Channel Scalar Form-factor

WEI LIU, HANQING ZHENG AND XIAO-LIN CHEN

*1) Department of Physics, Peking University, Beijing 100871, P. R. China*

## Abstract

A numerical analysis to the scalar form-factor in the  $\pi\pi$  and  $KK$  coupled–channel system is made by solving the coupled-channel dispersive integral equations, using the iteration method. The solutions are found not unique. Physical application to the  $\pi\pi$  central production in the  $pp \rightarrow pp\pi\pi$  process is discussed based upon the numerical solutions we found.

PACS numbers: 14.40.Aq; 11.55.Fv; 13.75.Lb

The  $I=J=0$  channel  $\pi\pi$  interactions are of great physical interests. Because the interaction of the  $I=J=0$  channel is very strong, the input bare singularities for a given model can be severely renormalized and distorted by the strong attractive force and extra dynamical singularities may be generated [1]. Therefore the  $I=J=0$  channel affords an ideal test ground for models of strong interactions. Also, the lightest glueball is expected to lie in the  $I=J=0$  channel, as predicted by the lattice QCD calculations. Therefore a detailed study to the dynamics in this channel becomes especially interesting. The low energy  $I=J=0$   $\pi\pi$  system manifests itself in various production processes intensively measured by experiments, *i.e.*, from  $\pi N \rightarrow \pi\pi N$ ,  $\gamma\gamma \rightarrow \pi\pi$  to  $J/\Psi \rightarrow \phi\pi\pi$ , etc., with the center of mass energy,  $\sqrt{s}$ , ranging from the  $\pi\pi$  threshold to a few GeV. When  $\sqrt{s}$  exceeds the  $KK$  threshold, a

single-channel analysis to the  $\pi\pi$  system becomes inadequate, and instead, a coupled-channel analysis of  $\pi\pi$  and  $K\bar{K}$  system has to be made. Among various  $\pi\pi$  production processes particularly interesting cases are those  $I=J=0$  final states which are generated weakly. In such circumstances, the final state particles will not scatter back to the initial states, and therefore the complicated dynamics involved is considerably simplified without loss of information on the  $I=J=0$  final state interactions. For example, in such a case the Watson–Migdal’s theorem on final state interactions applies. The  $\pi\pi$  final states “weakly” produced can be again categorized into two classes: One is that the  $\pi\pi$  production vertex contains left-hand singularities like in the case  $\gamma\gamma \rightarrow \pi\pi$ <sup>1</sup> and the another is not, like in the case  $K \rightarrow \pi\pi$  and in the  $\pi\pi$  central production process  $pp \rightarrow pp\pi\pi$ . Physical situation in the absence of left hand singularities is further simplified, since the dynamical complexity from the production vertex is removed which would otherwise disturb our analysis on the  $\pi\pi$  (final state) interaction itself. In such a simplified situation, it then becomes reasonable to assume that the  $\pi\pi$  production amplitude is factorized as a product of a form-factor-like quantity, which we denote as  $A$ , containing all the dynamical singularities from the right-hand cut from  $\pi\pi$  final state interactions, and the production vertex which is a smooth analytic function of  $s$  on the complex  $s$ -plane except possibly at infinity since it contains neither the left-hand nor the right-hand singularities.

For a coupled-channel system of  $\pi\pi$  and  $KK$ , the spectral representation of the form-factor,  $\mathbf{A} \equiv (A_1, A_2)$ , satisfies the following relation,

$$\begin{aligned}\text{Im}A_1 &= A_1\rho_1 T_{11}^+ + A_2\rho_2 T_{21}^+, \\ \text{Im}A_2 &= A_2\rho_2 T_{22}^+ + A_1\rho_1 T_{12}^+, \end{aligned}\tag{1}$$

whereas the unitarity relation of the scattering matrix  $\mathbf{T}$  reads,

$$\text{Im}\mathbf{T} = \mathbf{T}\rho\mathbf{T}^+, \tag{2}$$

where  $\rho \equiv \text{diag}(\rho_1, \rho_2)$  is the matrix of the kinetic phase-space factor. The  $\mathbf{T}$  matrix may contain left-hand cut but  $\mathbf{A}$  does not. Especially,  $\mathbf{A}$  is analytic on the entire physical sheet of the complex  $s$  plane except on the cut along the real positive axis starting from  $2\pi$  threshold. The form-factor  $\mathbf{A}$  has the same analytic structure as the scalar form-factor<sup>2</sup> and the two are different

---

<sup>1</sup>A recent publication on related subject can be found in Ref. [2].

<sup>2</sup>For the definition of the scalar form-factor, see for example Ref. [2].

only up to a polynomial. Eqs. (1) and (2) are assumed to be correct down to the lowest threshold, in the absence of anomalous thresholds. That means when  $4m_\pi^2 \leq s \leq 4m_K^2$  Eq. (1) takes the form,

$$\begin{aligned} \text{Im}A_1 &= A_1\rho_1 T_{11}^+ , \\ \text{Im}A_2 &= A_1\rho_1 T_{12}^+ . \end{aligned} \quad (3)$$

From previous discussions, it is realized that the physical problem of studying final state interactions in the production process without left-hand singularities is reduced to the mathematical problem of solving Eq. (1) (and Eq. (3)), provided that the  $\mathbf{T}$  matrix is known. In the single channel case the analytic solution of the form factor can be obtained. The spectral representation of the form-factor is given by the first equation in Eq. (3) from which the classical Omnès solution can be established,

$$A(s) = P(s) \exp \left( \frac{s}{\pi} \int_{4m_\pi^2}^\infty \frac{\delta_\pi(s')}{s'(s' - s - i\epsilon)} ds' \right) , \quad (4)$$

where  $P(s)$  is a polynomial and  $\delta_\pi$  is the  $\pi\pi$  scattering phase. The Omnès solution is remarkable in relating the form-factor to  $\delta_\pi$ . The Eq. (4) has been used in Ref. [3] to study the final state interactions in  $K \rightarrow 2\pi$  and  $pp \rightarrow pp\pi\pi$  systems. In the coupled-channel case, however, no analytic solutions of Eq. (1) can be obtained in general. In the following we will instead study the coupled-channel system by numerical method [4].

Since the coupled-channel form-factor  $\mathbf{A}$  is analytic on the physical sheet of the complex  $s$  plane except for the cut along the real axis, assuming the  $\mathbf{T}$  matrix is known we can search for solutions of the amplitude  $\mathbf{A}$  in Eq. (1) by solving the following dispersion relation:

$$\mathbf{A} = \frac{1}{\pi} \int_R \frac{\mathbf{A}\rho\mathbf{T}^+(s')}{s' - s - i\epsilon} ds' , \quad (5)$$

where the integration is performed on the unitarity cut  $R$ , starting from  $4m_\pi^2$  to  $\infty$ . The Eq. (5), according to Muskhelishvili [5], contains two fundamental solutions,  $\phi_1$  and  $\phi_2$ . Assuming that  $\phi_n$  behaves as  $\phi_n \rightarrow s^{-\chi_n}$  as  $s \rightarrow \infty$  one has

$$\sum_n \chi_n = \frac{1}{2\pi} [\arg \det \mathbf{S}]_R = \frac{1}{\pi} (\delta_\pi(\infty) + \delta_K(\infty)) , \quad (6)$$

where  $\mathbf{S}$  is the coupled-channel  $S$  matrix. According to [5], any solution of the integral equation (5) can be written as a linear composition of the two fundamental solutions,

$$\phi = \sum_n P_n(s) \phi_n \quad , \quad n = 1, 2 \quad (7)$$

where  $P_n(s)$  are polynomials of  $s$ . The polynomials are not determined from analyticity alone. Other physical input has to be implemented to fix their coefficients. For example, chiral perturbation theory can afford an expansion of the scalar form-factor in powers of  $s$  when  $s$  is small [6]. Since there can be many solutions of Eq. (5) and we notice that, since the numerical integration in Eq. (5) has to be truncated somewhere (denoted as  $\Lambda$  below), all the information on the asymptotic behaviour are lost. As a consequence, it is difficult to distinguish the so-called fundamental solutions from others, since the difference between the two essentially comes from their asymptotic behaviours. Therefore in the present numerical scheme instead of searching for the fundamental solutions, we follow the recipe of Ref. [4], that is to search for two linearly independent solutions,  $\mathbf{A}^1$  and  $\mathbf{A}^2$  which are normalized at  $s = 0$  as,

$$A_1^1(0) = 1 \quad , \quad A_2^1(0) = 0 \quad , \quad (8)$$

and

$$A_1^2(0) = 0 \quad , \quad A_2^2(0) = 1 \quad . \quad (9)$$

In the following we use the  $\pi\pi$  and  $KK$  coupled-channel fit of the T matrix from Au, Morgen and Pennington [7] as an educative example to solve the coupled-channel dispersive integral equation (5). The integral in Eq. (5) is truncated at  $\Lambda \simeq 1.5 GeV$ . We find that the influence of the cutoff is rather local, i.e., it has little effects on the behaviour of the solution in a large region of  $s$ , even close to  $\Lambda$ . One can also use a mild regulation function instead of the truncation at  $\Lambda$  and the result is essentially the same except at  $s \simeq \Lambda$ . We use the iteration method to solve Eq. (5). That is,

$$\mathbf{A}^{(n+1)}(s) = \mathbf{A}(0) + \frac{s}{\pi} \int_{4m_\pi^2}^\Lambda \frac{\text{Real} [\mathbf{A}^{(n)}(\mathbf{s}') \rho \mathbf{T}^+(s')]}{s'(s' - s - i\epsilon)} ds' \quad , \quad (10)$$

where

$$\mathbf{A}(0) = (1, 0) \quad \text{or} \quad (0, 1) \quad . \quad (11)$$

A once-subtracted form of the dispersive integral in the above Eq. (10) is helpful in incorporating the boundary conditions, Eqs. (8) and (9). The routine converges rather rapidly (after about 20 steps), which confirms the claim in Ref. [4] and the solutions are not unique due to the reason already mentioned above. This means that the iteration may converge to different solutions depending on different initial values for the iteration. In Fig. 1 and Fig. 2 a few examples generated from our numerical recipe are shown. We see from Fig. 1 that all the phases are identical to the phase of  $T_{11}$  below the  $K\bar{K}$  threshold as required by the final state theorem. Above the  $K\bar{K}$  threshold, however, the phases from different solutions of  $A_1$  can be very different and also deviate from the phase of  $T_{11}$ . In Fig. 2 the corresponding magnitude of the different solutions is also shown. We see that around  $1GeV$  region there can be zeros or dips to compensate the peak generated by  $f_0(980)$ . The physical discussion on the necessity to introduce the protective zero appearing in the  $\pi\pi$  production processes can be found in Ref. [3, 9]. In the present numerical approach there is generally no difficulty to pick suitable solutions, from all, to fit experimental data. An example is shown in Fig. 3 where the  $\pi\pi$  production cross-section in the  $pp \rightarrow pp\pi\pi$  process is reproduced. The cross-section can be expressed by [10],

$$\frac{d\sigma}{d\sqrt{s}} \sim \frac{(s - 4m_\pi^2)^{1/2}}{s^{3/2}} |F(s)|^2 , \quad (12)$$

where  $F(s)$  is a linear combination of solutions  $A_1^1$  and  $A_1^2$ ,

$$F(s) = \alpha_1 A_1^1 + \alpha_2 A_1^2 . \quad (13)$$

It is assumed here that  $\pi\pi$  produced in the  $pp \rightarrow pp\pi\pi$  process are generated from the fusion of Pomeron pairs and no left-hand singularity is involved in the production vertex. Therefore  $\alpha_1$  and  $\alpha_2$  (which contain information about the  $\pi\pi$  production vertex) appearing in the above equation are expected to be polynomials with a weak dependence on  $s$ .

In fact, the T matrix given in Ref. [7] is obtained by a multi-pole K matrix fit in which the background effects including the left-hand cut one are simulated by a polynomial. Therefore, the T matrix does not contain any left-hand singularity. Under such an approximation it is not really necessary to search for the numerical solutions of  $A_1$  in order to make use of Eq. (13). Since  $A_1$  has to be a linear combination of  $T_{11}$  and  $T_{21}$  when neglecting the

left-hand singularities in  $T$ , one can use instead of Eq. (13) the following form,

$$F(s) = \alpha'_1 T_{11} + \alpha'_2 T_{21}, \quad (14)$$

to fit the experimental data, as originally done in Ref. [7]. The method presented in the current note applies to more general cases when the fine details of the left-hand singularities of the scattering  $T$  matrix are carefully taken into account. Also our program can be easily extended to the situation when the left-hand cut of the production vertex is included. We will investigate these more realistic cases in future.

**Acknowledgement:** One of the authors, H.Z. would like to thank M. Locher and V. Markushin for helpful discussions. He is supported in part by National Natural Science Foundation of China under grant No. 19775005.

## References

- [1] See for example, M. P. Locher, V. E. Markushin and H. Q. Zheng, Eur. Phys. J. **C4**, 317(1998) and references therein.
- [2] Ulf-G. Meißner and J. A. Oller, Preprint hep-ph/0005253.
- [3] M. Locher, V. Markushin and H. Zheng, Phys. Rev. **D55**, 2894(1997)
- [4] Similar approach has been discussed by, J. F. Donoghue, J. Gasser and H. Leutwyler, Nucl. Phys. **B343**, 341(1990).
- [5] N. I. Muskhelishvili, *Singular Integral Equations*, Moscow, 1946.
- [6] J. Gasser and U. G. Meißner Nucl. Phys. **B357**, 90(1991);
- [7] K. L. Au, D. Morgan and M. R. Pennington, Phys. Rev. **D35**, 1633(1987).
- [8] T. Akesson *et al.* Nucl. Phys. **B264**, 154(1986).
- [9] M. Locher, V. Markushin and H. Zheng, Phys. Rev. **D58**, 038504(1998); D. Morgan and M. R. Pennington, Phys. Rev. **D58** (1998) 038503;
- [10] D. Morgan and M. R. Pennington, Phys. Lett. **137B** (1984) 411.

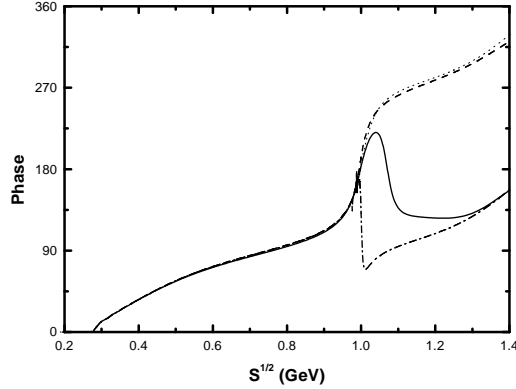


Figure 1: The solid, dashed and dot-dashed lines represent the phases of different solutions of the  $A_1^1$  amplitudes, the corresponding magnitude of the amplitudes are depicted in Fig. 2. The dotted line represents the phase of  $T_{11}$  from the K3 fit of Ref. [7].

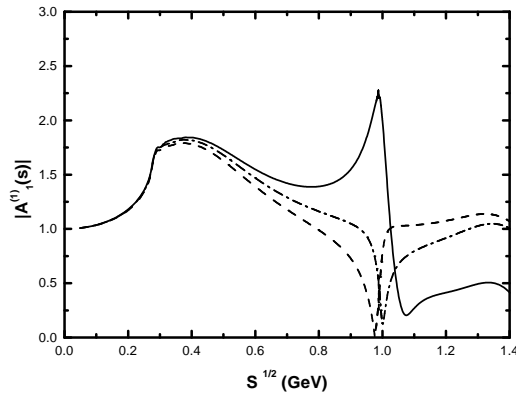


Figure 2: The magnitude of the different solutions of the  $A_1^1$  amplitude.

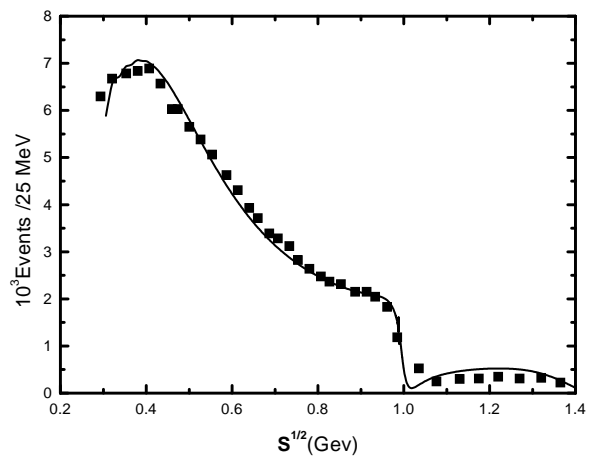


Figure 3: The effective mass distribution of pion pairs in  $pp \rightarrow pp\pi\pi$  vs.  $M = \sqrt{s}$ . The data are from [8].